



The Complex Crystal Structure and Abundant Local Defects of Zeolite EMM-17 Unraveled by Combined Electron Crystallography and Microscopy

Xiaona Liu⁺, Lingmei Liu⁺, Tingting Pan, Nana Yan, Xinglong Dong, Yuanhao Li, Lu Chen, Peng Tian, Yu Han,^{*} Peng Guo,^{*} and Zhongmin Liu

Abstract: In this study, we successfully solve polymorphs A and B of zeolite EMM-17, which can only crystallize in sub-micrometer-sized crystals while containing complex stacking disorders, from the three-dimensional (3D) electron diffraction (ED) data. This is the first time that the atomic structure of this polymorph has been *ab initio* solved, and the result reveals a unique $10(12) \times 10(12) \times 11$ -ring channel system. Moreover, we acquire the first atomic-resolution images of EMM-17 using integrated differential phase-contrast scanning transmission electron microscopy. The images allow us to directly observe polymorphs B and C and discover a large number of local structural defects. Based on structural features unraveled from the reciprocal-space 3D ED data and real-space images, we propose a series of energetically feasible local structures in EMM-17. We also demonstrate that the unique porous structure of EMM-17 enables efficient kinetic separation of C_6 alkane isomers.

Introduction

Zeolites are a class of microporous crystalline materials with well-defined cavities and channels of molecular dimensions. Their most intriguing feature is the molecular sieving ability, which enables them to separate gas mixtures and catalyze reactions with unique size-/shape-selectivity.^[1–4] The properties of a given zeolite depend mainly on its crystallographic structure, i.e., how the structural building units, TO_4 tetrahedra (T = Si, Al, Ti, etc.), are connected to construct a periodic framework. Solving the crystal structure of a novel zeolite is therefore a crucial step towards understanding its structure-property correlations and developing its applications.^[5–8] Furthermore, zeolite crystals often contain a variety

of non-periodic local structural features, such as crystal surfaces, grain boundaries, stacking disorders, and point/line defects, which also have important effects on their performances.^[9]

Single crystal X-ray diffraction (SC-XRD) is the first choice for solving the structures of zeolites. Unfortunately, many zeolites can only grow into submicron crystals that are too small to be studied by SC-XRD. Powder X-ray diffraction (PXRD) can also be used, but the one-dimensional diffraction data of PXRD often encounters the situation where the diffraction peaks overlap severely and/or there are multiple phases or impurities, which leads to the failure of structure solution. For a complex zeolite structure, it is sometimes even challenging to determine unit cell parameters using PXRD, which is the first step for the structure solution.^[10,11]

Transmission electron microscopy (TEM) that combines electron diffraction (ED) in reciprocal space and direct imaging in real space has proven to be a powerful tool for investigating zeolitic structures. In comparison with X-ray diffraction, TEM has advantages in two aspects. On the one hand, electron diffraction can be implemented on a single nano-sized crystal, due to the ease of manipulation of the electron beam and the strong electron-matter interaction. The rotation electron diffraction (RED) technique allows the collection of three-dimensional (3D) ED datasets, which are equivalent to SC-XRD datasets and can therefore be used to solve crystal structures using established phasing algorithms. In this sense, RED is a single-crystal diffractometer for nano-sized crystals.^[12,13] The latest development of this technique, called continuous rotation electron diffraction (cRED), enables the collection of datasets in a continuous manner in a very short period of time, which is essential for preserving

[*] X. Liu,^[†] N. Yan, Y. Li, P. Tian, P. Guo, Z. Liu

National Engineering Laboratory for Methanol to Olefins, State Energy Low Carbon Catalysis and Engineering R&D Center, Dalian National Laboratory for Clean Energy, Dalian Institute of Chemical Physics, Chinese Academy of Sciences
 Dalian 116023, Liaoning (P. R. China)
 E-mail: pguo@dicp.ac.cn

X. Liu,^[†] Y. Li, Z. Liu
 University of Chinese Academy of Sciences
 Beijing 100049, Beijing (P. R. China)
 L. Liu^[†]



Multi-scale Porous Materials Center, Institute of Advanced Interdisciplinary Studies & School of Chemistry and Chemical Engineering, Chongqing University
 Chongqing 400044 (P. R. China)

T. Pan, X. Dong, Y. Han

Advanced Membranes and Porous Materials Center, Physical Sciences and Engineering Division
 King Abdullah University of Science and Technology
 Thuwal, 23955-6900 (Saudi Arabia)
 E-mail: yu.han@kaust.edu.sa

L. Chen
 Thermo Fisher Scientific (China) Co., Ltd.
 Shanghai 201203, Shanghai (P. R. China)

[†] These authors contributed equally to this work.

 Supporting information and the ORCID identification number(s) for the author(s) of this article can be found under:
 <https://doi.org/10.1002/anie.202109957>.

the crystal structure of electron beam-sensitive materials such as zeolites.^[14] With cRED, the data quality has also been significantly improved due to the 3D integration of diffraction intensities and the reduction of collection time and total electron dose. On the other hand, TEM can generate real-space images with atomic resolution, which not only contain information of “structure factors” but also directly display local structural features that are not visible by diffraction-based techniques.^[6,15–17] Because the contrast of conventional high-resolution TEM (HRTEM) image is related to the imaging conditions, especially the defocus value of the objective lens, it is difficult to interpret.^[18] Compared with HRTEM, the emerging integrated differential phase-contrast scanning transmission electron microscopy (iDPC-STEM) imaging mode has the advantage of producing easy-to-interpret images and it can image heavy and light elements simultaneously.^[19,20]

In addition to small crystal sizes, some zeolites have stacking disorders, which cause diffuse scatterings in diffraction, thus making their structural elucidation even more challenging. Zeolite Beta (***BEA**) is a typical example, whose structure was finally solved through the combination of structural modeling and multiple characterization techniques in 1998, when its synthesis had been reported for more than 20 years.^[21–23] Other zeolites with such stacking disorders were mainly solved by structural modeling based on the HRTEM images, such as SSZ-26 and SSZ-33 (**CON**), SSZ-31 (***STO**), and ETS-10.^[24–26] There are also a few zeolite structures determined from HRTEM images solely, such as ITQ-39 (***ITN**) and ECNU-5 (***SVY**).^[6,15] EMM-17 is another zeolite with stacking disorders, which was invented by ExxonMobil in 2012.^[27] In 2019, Weston et al. delicately deduced the structure of EMM-17 from a related zeolite NU-86^[28] through modeling and verified it using DIFFaX simulation.^[29] However, a direct ab initio structure determination of EMM-17 has not been achieved, and DIFFaX simulations cannot probe local structural defects that are commonly found in zeolites.

In this work, we solved polymorphs A and B in EMM-17 directly from the cRED dataset, without the need of assuming an initial model. The results reveal that EMM-17 has a unique 3D 10(12) × 10(12) × 11-ring channel system, which is consistent with the pioneering work of Weston et al. Using iDPC-STEM, we further discovered the existence of a large number of structural defects in EMM-17, including various polymorphs and abnormal 8-ring pore openings, distributed throughout the framework. These observations allow us to predict a series of energetically feasible structures. In addition, we demonstrated that EMM-17 has great potential in the separation of linear and branched C₆ alkane isomers.

Results and Discussion

Pure-silica EMM-17 was synthesized by using 1-methyl-4-(pyrrolidin-1-yl) pyridine-1-ium hydroxide (MePPyOH) as the organic structure-directing agent (OSDA), according to the method reported in the patent from ExxonMobil.^[27] SEM image shows that EMM-17 consists of sub-micron-sized

crystals with a plate-like morphology (Figure S1). EMM-17 exhibits a type I Ar sorption isotherm at 87 K (Figure S2), which reveals its microporous nature. The PXRD pattern shows both sharp and broad peaks (Figure S3), indicating that stacking disorders might be present in the structure. Consequently, it is hardly possible to determine its crystallographic structure by employing conventional approaches.

To solve the complex structure of EMM-17, we first collected a high-quality 3D ED dataset (resolution: 0.85 Å; completeness: 87.8%; 825 ED frames ranging from –59.1° to 61.8°) within three minutes using the cRED technique (Table S1). The reconstructed reciprocal lattice clearly shows diffuse scatterings (Figure 1 a and b), which is consistent with observations in PXRD. This phenomenon implies the coexistence of polymorphic structures in EMM-17, which corresponds to the different stacking modes. We pinpointed the intensity maximums in the diffraction streaks by following the reciprocal lattice established according to the sharp, non-diffuse reflections. The extracted points were indexed with an orthorhombic unit cell: $a = 24.7$ Å, $b = 23.3$ Å, $c = 12.4$ Å, and the possible space groups were deduced to be $P2_12_12$ and $P2_122$ according to the reflection conditions (Figure 1 b–d). Then, we applied the direct methods implemented in SHELXT to the cRED dataset and successfully solved the structure with the space group of $P2_12_12$. As shown in Figure 2 a, all 30 T atoms and 58 out of 61 O atoms in the asymmetric unit were clearly resolved, and the three missing O atoms could be identified after one-cycle refinement against the cRED data. The resolved structure represents the primary polymorph of EMM-17 and is denoted as polymorph A. Notably, the structure of another main

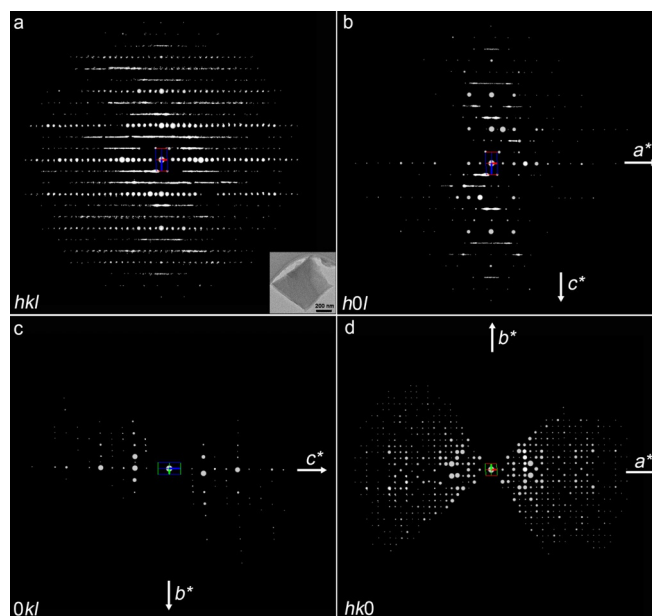


Figure 1. a) Reconstructed 3D reciprocal lattice of EMM-17 from the cRED data. Inset is the TEM image of the crystal from which the cRED data was collected. b)–d) Three two-dimensional slices $h0l$, OkI , and $hk0$ extracted from the reconstructed reciprocal lattice. Reflection conditions: $h00$: $h = 2n$. The possible space groups are $P2_12_12$ and $P2_122$.

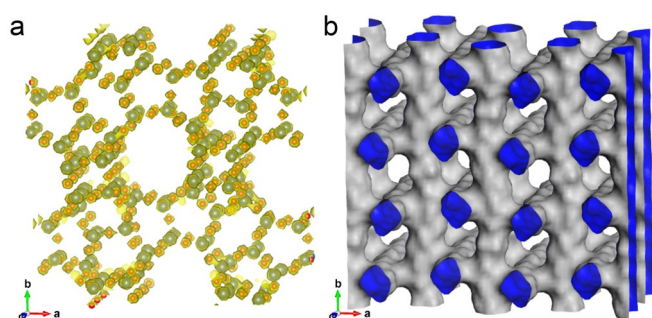


Figure 2. a) 3D electrostatic potential map of EMM-17 polymorph A. The solved T and O atoms are represented by green and orange balls, respectively and superimposed in the potential map. b) 3D channel system of EMM-17 polymorph A.

polymorph (polymorph B) of EMM-17 can also be determined from the same cRED dataset in a similar way, but using a monoclinic lattice ($a = 25.3 \text{ \AA}$, $b = 22.0 \text{ \AA}$, $c = 12.4 \text{ \AA}$, $\beta = 99.8^\circ$) to pinpoint reflections from the streaks (see Figures S4 and S5). Among the zeolites that have been studied by cRED, PST-24 and EMM-25 contain disorders,^[8,30] but they have only 11 and 10 T atoms in the asymmetric unit, respectively (see Table S2). In comparison, the structural solution of EMM-17 is more challenging, as it requires collecting more reflections with reliable intensities. In addition, we demonstrated that the way we process the 3D ED data containing diffuse scattering can be used as a general strategy for the structure determination of other zeolites with stacking disorders, such as zeolite Beta (*BEA) (Figures S6 and S7; Tables S1 and S3).

The resolved structure shows that polymorph A contains zigzag channels with alternating 10- and 12-ring pore openings along the a -axis, straight channels with alternating 10-ring and 12-ring pore openings along the b -axis, and unusual straight 11-ring channels along the c -axis (Figure 2b). Hence, the structure of EMM-17 is characterized by a complex 3D channel system designated as $10(12) \times 10(12) \times 11$ -rings. It is

worth noting that there are very few zeolites having 11-membered rings, including gallogermanate JU-64, germanosilicate PKU-16, borosilicate EMM-25, aluminosilicate PST-31, and aluminosilicate NU-86.^[28,30–33] JU-64 and PKU-16 are unstable upon the removal of OSDAs. To our knowledge, EMM-17 is the only 11-ring zeolite that can be synthesized in both aluminosilicate and silicate forms. Importantly, its structure is highly stable under thermal and hydrothermal conditions (Figure S3), which means that its unique 11-ring channels are fully accessible and useful for separation and catalysis.

The framework of EMM-17 can be considered to be constructed from two basic structural motifs, namely, “butterfly” and “5-6-5-6”, which have been identified in the *BEA and SOV/POS frameworks, respectively.^[22,23,31,34] Alternate connection of the “butterfly” and “5-6-5-6” motifs by sharing 4-rings results in the formation of a chain of composite building units (CBU) along the b -axis (Figure 3a). Further connection of the CBU chains along the c -axis leads to the formation of a planar building unit (denoted as EMM-17 building layer 1) in the bc -plane (Figure 3b and Figure 5a). As illustrated in Figure S8, applying rotation and translation operations to the EMM-17 building layer 1 generates another building unit (denoted as EMM-17 building layer 2). Alternate stacking of EMM-17 building layer 1 and EMM-17 building layer 2 along the a^* -axis produces the 3D framework of EMM-17, and different polymorphs are formed depending on the stacking mode. When the adjacent building layers shift $+1/3 c$, $-1/3 c \dots$ or $+1/3 c$, $+1/3 c \dots$ in succession, resulting in ABAB... or ABCABC... stacking sequence, polymorph A and polymorph B are formed, respectively (Figures 3c and d). This explains the sharp spots observed in every third line in the two-dimensional reciprocal lattice (Figure 1b and Figure S9b).^[35] If building layers stack along a^* -axis without any translations along the c -axis, polymorph C of EMM-17 with an AA... stacking sequence is generated (Figure 3e). All the three types of polymorphs have the same projection along the

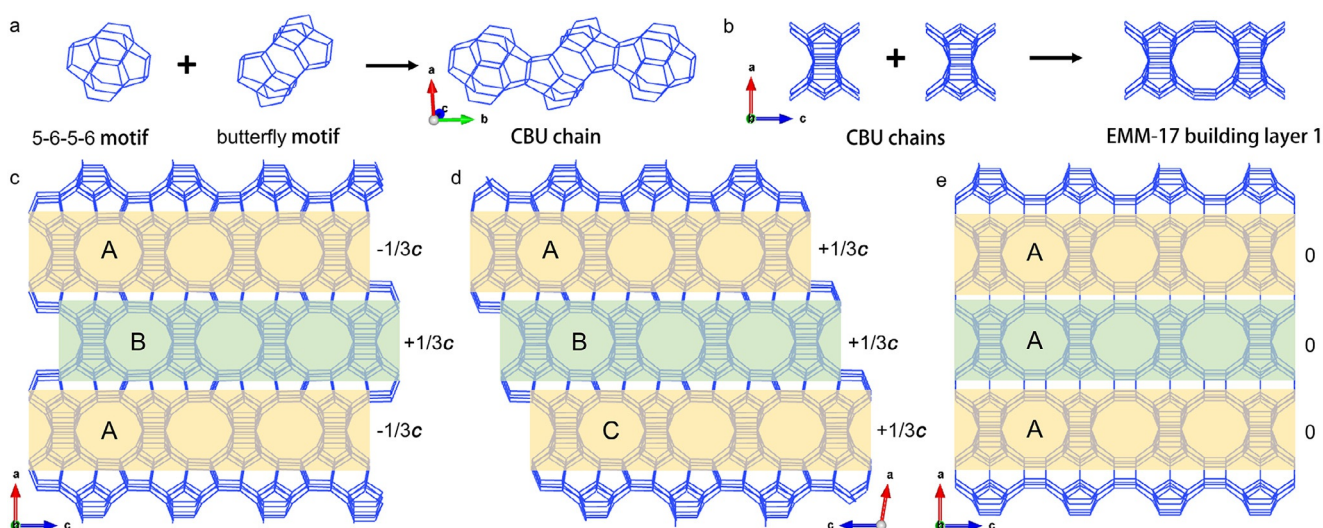


Figure 3. a) The construction of a CBU chain from 5-6-5-6 and butterfly motifs. b) The formation of “EMM-17 building layer 1” by connecting CBU chains along the c -axis. c)–e) Polymorphs A, B, and C of EMM-17. EMM-17 building layer 1 and EMM-17 building layer 2 are highlighted in orange and green, respectively.

c-axis (11-ring channels), while stacking disorders occur in the *ac*-plane, and their atomic coordinates are listed in Table S3.

We further probed the non-periodic and local structures in EMM-17 by real-space electron microscopy imaging. HRTEM images clearly show the characteristic 11-ring channels along the *c*-axis and the coexistence of polymorphs A and B along the *b*-axis (Figure S9), which is fully consistent with the structure model solved from the 3D cRED data. However, image processing or simulation is required to make the HRTEM images interpretable at the atomic resolution. In order to avoid these tedious processes, we mainly used iDPC-STEM for the study, given that the contrast of iDPC-STEM image can be approximately interpreted as the local electrostatic potential field of the thin specimen.^[36,37] Figure 4a shows the high-resolution iDPC-STEM image of EMM-17 acquired along the *c*-axis, in which the unique 11-ring channels and alternating arrangement of “butterfly” and “5-6-5-6” motifs are directly observed. In good agreement with our structural model, intergrowth of polymorphs A and B is frequently observed in the image acquired along the *b*-axis (Figures 4b and c). The presence of polymorph C is also found in some small areas (Figure 4b). In view of the very low content of polymorph C observed, we simulated the PXRD pattern of EMM-17 based on the coexistence of polymorph A and polymorph B (50:50) using the DIFFaX software.^[38] The simulated PXRD pattern showed a fairly good match with the experimental one (Figure S10). Most interestingly, the iDPC-STEM images reveal unprecedented types of structural

defects in EMM-17 (Figure 4b and c). One typical defective structure is featured by an elliptical 8-ring pore opening, as illustrated in Figure 4d. The formation of this defect can be understood as: when two CBU chains meet along the *c*-axis, they do not adopt the direct connection manner usually observed in the bulk structure (Figure 5a), but merge by eliminating two T atoms, thereby resulting in a smaller pore opening (Figure 5b). Another typical defective structure is formed by the complete fusion of two CBU chains into a compact (nonporous) structural moiety, as illustrated in Figure 4e. Such compact structural moieties contain Q₃ Si species, which is consistent with the results of ²⁹Si MAS NMR and ¹H-²⁹Si CP MAS NMR (Figure S11).

There are more complex defects existing in EMM-17, as indicated by the local abnormal image contrast, but their structures cannot be conclusively determined. The abnormal image contrast presented in Figure 4f can be explained as a number of elliptical 8-ring moieties connected in series along the *c*-axis. The abnormal image contrast presented in Figure 4g can be attributed to the coexistence of polymorph B and polymorph C domains along the projection direction (the *b*-axis) that are offset along the *c*-axis. This type of connection would also lead to the generation of Q₃ Si species, which are marked in red in the structural model (Figure 4g). It is worth noting that the proposed defective structures also have 11-ring channels running along the *c*-axis (Figures 4h and i).

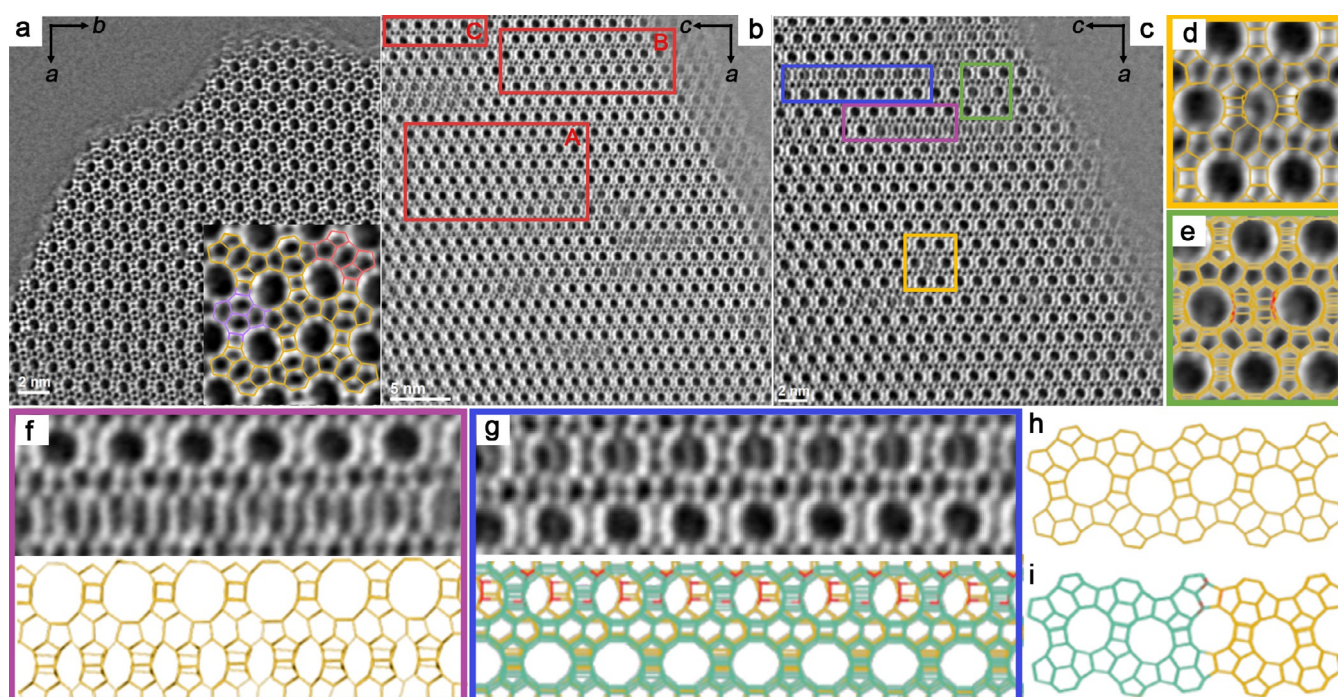


Figure 4. iDPC-STEM images of calcined EMM-17 taken along the a) *c*- and b) *b*-axis. The insert picture in (a) is the enlarged image with the zeolite framework model superimposed, in which the butterfly and 5-6-5-6 motifs are highlighted in pink and lilac, respectively. Typical regions of polymorphs A, B, and C are marked in (b). d)–g) The enlarged view of various local defects observed in (c), along with the proposed structural models. The enlarged images and the selected areas are correlated by the labelling colors. h), i) The structural models in (f) and (g) viewed along the *c*-axis, respectively. In (g) and (i), polymorphs B and C are shown in orange and turquoise, respectively. In (e), (g), and (i), the Q₃ T atoms are highlighted in red.

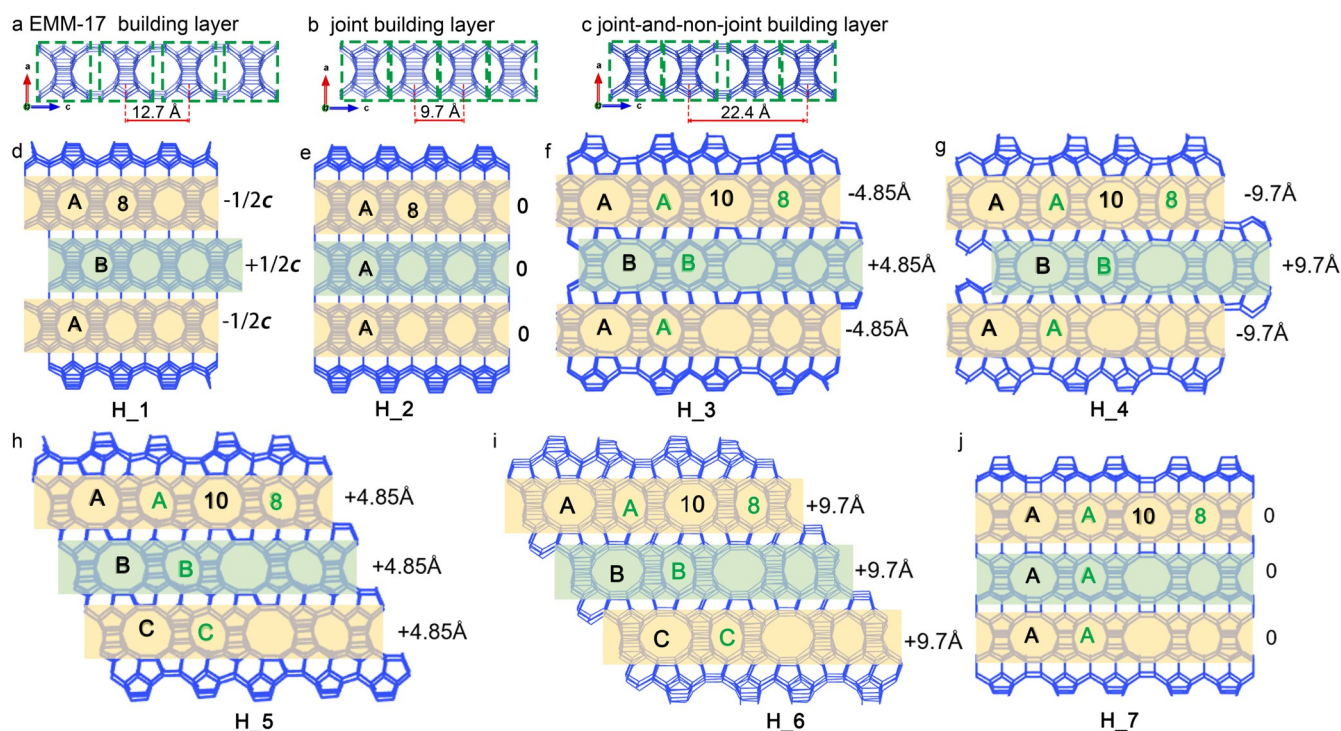


Figure 5. a)–c) Three building layers constructed by the CBU chains. The CBU chains are labelled by green rectangles. d), e) H₁ and H₂ constructed from the joint building layer. f)–j) H₃, H₄, H₅, H₆ and H₇ built by joint-and-non-joint layer. The corresponding building layer 1 and building layer 2 are highlighted in orange and green, respectively.

Inspired by the abundant and diverse non-periodic defective structures observed in iDPC-STEM images, we further built a series of energetically and topologically feasible hypothetical structures. Three possible building layers have been identified, which are all based on the connection of CBU chains along the *c*-axis, but in different manners. They are designated as “EMM-17 building layer”, “joint building layer”, and “joint-and-non-joint building layer”, respectively (Figures 5 a, b, and c).

1) If the adjacent joint building layers shift $+1/2c$, $-1/2c$... or do not shift along *c*-axis and then stack along the *a**-axis, two hypothetical structures denoted as H₁ and H₂ with ABAB... and AA... stacking sequence will be constructed (Figures 5 d,e, and Figure S12).

2) If the adjacent joint-and-non-joint building layers shift one or half of CBU chain width (9.7 Å) or do not shift along the *c*-axis and then stack along the *a**-axis, another five hypothetical structures (H₃–H₇) with ABAB..., ABCAB..., AA... stacking sequences can be logically built (Figures 5 f–j and Figure S13).

All these seven hypothetical structures have unique elliptical 8-ring pore openings, and their structural details are described in Table S4.

The unique 10/11/12-rings porous structure endows EMM-17 with a micropore size (4–7 Å) (Figure S14), which is in the range of the kinetic diameters of C₆ alkane isomers: n-hexane (nHEX, 4.3 Å), 3-methylpentane (3MP, 5.0 Å), and 2,2-dimethylbutane (22DMB, 6.2 Å).^[39] We measured vapor adsorption isotherms of EMM-17 for nHEX, 3MP, and 22DMB at 25 °C. For these three C₆ isomers, EMM-17

showed typical type I isotherms with similar equilibrium adsorption capacities (Figure 6a). However, the adsorption kinetics measurement conducted at 25 °C and 1 mbar showed that as the kinetic diameter of the isomer increased, the molecular diffusion in EMM-17 became slower, and their diffusion time constants (D/r^2) were determined to be 0.00414, 0.00307, and 0.00163 s⁻¹, respectively (Figure 6b). These single-component vapor adsorption results suggest that EMM-17 is a promising adsorbent that can be used for the kinetic separation of the C₆ alkane isomers.

To verify the separation ability of EMM-17, we performed column breakthrough experiments with a ternary mixture of equimolar nHEX, 3MP, and 22DMB (see the SI for experimental details). The results show that EMM-17 can well separate these isomers: 22DMB first eluted from the column, which was followed by 3MP, while nHEX that can most easily diffuse into the pore system of EMM-17 was retained in the column for the longest time. Specifically, under our testing conditions, the breakthrough times are 32, 49, and 77 min for 22DMB, 3MP, and nHEX, respectively (Figure 6c). To gain more insights into the separation mechanism, we collected the adsorption isotherms of the three isomers on EMM-17 at 180, 200, and 220 °C (Figure S15). Using the Clausius-Clapeyron equation, the isosteric heat of adsorption of nHEX, 3MP, and 22DMB were calculated to be 67.0, 67.2, and 68.5 kJ mol⁻¹, respectively. The small difference between the adsorption heats indicates that the excellent C₆ alkane separation ability of EMM-17 is mainly attributed to kinetic rather than thermodynamic factors. We believe that in addition to the primary pore structure of EMM-17, the presence of smaller

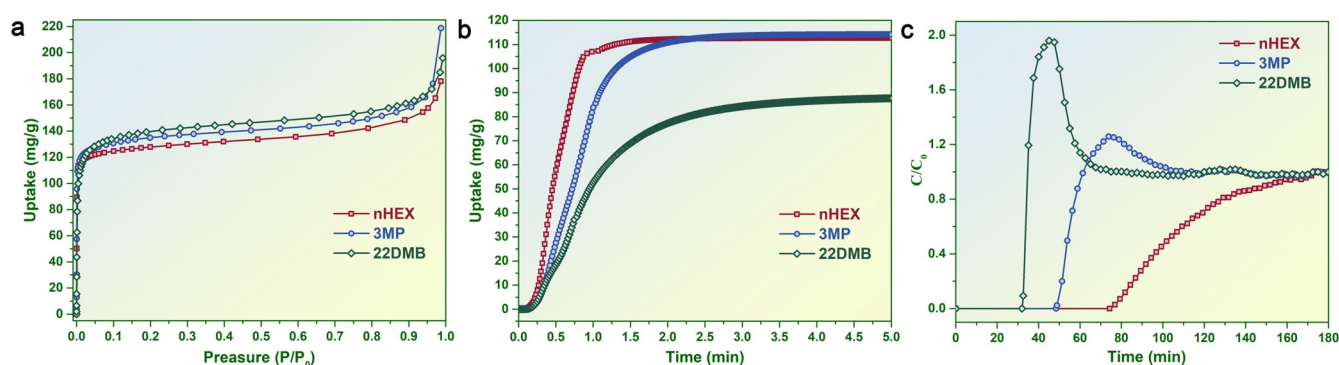


Figure 6. a) Adsorption isotherms and b) adsorption kinetics of EMM-17 for nHEX, 3MP, and 22DMB at 25 °C. The adsorption kinetics were measured at 1 mbar. c) Column breakthrough curves of a ternary mixture of nHEX, 3MP, and 22DMB on EMM-17 at 25 °C.

pore openings related to the abundant structural defectives imposes extra diffusion restrictions on larger molecules, thereby further enhancing the separation effect.

Conclusion

We successfully solved the structure of the new zeolite EMM-17, which is featured by a unique $10(12) \times 10(12) \times 11$ -ring channel system, using cRED. Although the crystal structure of EMM-17 solved by cRED is no different from that determined by the modeling method, this is the first ab initio structural solution of such a complex structure directly from the experimental data, without the need for prior knowledge or any assumptions. We proposed a general strategy to process 3D ED datasets with diffuse scattering and demonstrated its effectiveness in solving crystal structures having high degrees of stacking disorders. We used iDPC-STEM to probe the diverse local structures of EMM-17 and identified the structures of co-existing polymorphs as well as abundant structural defects. The combined reciprocal-space and real-space characterizations provide comprehensive structural information about this new member of zeolite family that will facilitate in-depth understanding of its properties. Based on the observed non-periodic structural features, we predicted a series of energetically and topologically feasible hypothetical structures. EMM-17 exhibits the ability to separate linear, monobranched and dibranched C_6 alkane isomers, and the separation is mainly controlled by kinetic factors.

Acknowledgements

This work is supported by the National Natural Science Foundation of China (No. 21972136, 21991090, and 21991091), the Pioneer Hundred Talents Program, Chinese Academy of Sciences (No. Y706071202), the Dalian National Laboratory for Clean Energy Cooperation Fund, Chinese Academy of Sciences (No. DNL201908), the Key Research Program of Frontier Sciences, Chinese Academy of Sciences (No. QYZDB-SSW-JSC040), and the Center Competitive Fund (CCF) to Y.H. from King Abdullah University of

Science and Technology, N.Y. acknowledges financial support from the CAS Special Research Assistant Program and the scholarship from STOE. We thank Dr. Lei Wang (Nanjing Tech University) for optimizing hypothetical structures. We thank the assistance from Professor Hao Wang at Hoffmann Institute of Advanced Materials about adsorption isotherms of nHEX, 3MP, and 22DMB at different temperatures. We also thank Yingjiang Lian from Dalian Institute of Chemical Physics for his assistance in the synthesis of OSDA.

Conflict of Interest

The authors declare no conflict of interest.

Keywords: C_6 isomer separation · electron crystallography · EMM-17 · zeolites

- [1] P. Tian, Y. Wei, M. Ye, Z. Liu, *ACS Catal.* **2015**, *5*, 1922–1938.
- [2] P. S. Barcia, J. A. C. Silva, A. E. Rodrigues, *Ind. Eng. Chem. Res.* **2006**, *45*, 4316–4328.
- [3] P. J. Bereciartua, . Cantın, A. Corma, J. L. Jorda, M. Palomino, F. Rey, S. Valencia, E. W. Corcoran, P. Kortunov, P. I. Ravikovitch, A. Burton, C. Yoon, Y. Wang, C. Paur, J. Guzman, A. R. Bishop, G. L. Casty, *Science* **2017**, *358*, 1068–1071.
- [4] A. Bhan, A. D. Allian, G. J. Sunley, D. J. Law, E. Iglesia, *J. Am. Chem. Soc.* **2007**, *129*, 4919–4924.
- [5] D. Jo, G. T. Park, J. Shin, S. B. Hong, *Angew. Chem. Int. Ed.* **2018**, *57*, 2199–2203; *Angew. Chem.* **2018**, *130*, 2221–2225.
- [6] T. Willhammar, J. Sun, W. Wan, P. Oleynikov, D. Zhang, X. Zou, M. Moliner, J. Gonzalez, C. Martınez, F. Rey, A. Corma, *Nat. Chem.* **2012**, *4*, 188–194.
- [7] M. O. Cichocka, Y. Lorgouilloux, S. Smeets, J. Su, W. Wan, P. Cautlet, N. Bats, L. B. McCusker, J.-L. Paillaud, X. Zou, *Cryst. Growth Des.* **2018**, *18*, 2441–2451.
- [8] D. Jo, J. Zhao, J. Cho, J. H. Lee, Y. Liu, C. Liu, X. Zou, S. B. Hong, *Angew. Chem. Int. Ed.* **2020**, *59*, 17691–17696; *Angew. Chem.* **2020**, *132*, 17844–17849.
- [9] K. Barbera, F. Bonino, S. Bordiga, T. V. W. Janssens, P. Beato, *J. Catal.* **2011**, *280*, 196–205.
- [10] P. Guo, J. Shin, A. G. Greenaway, J. G. Min, J. Su, H. J. Choi, L. Liu, P. A. Cox, S. B. Hong, P. A. Wright, X. D. Zou, *Nature* **2015**, *524*, 74–78.
- [11] F. Gramm, C. Baerlocher, L. B. McCusker, S. J. Warrender, P. A. Wright, B. Han, S. B. Hong, Z. Liu, T. Ohsuna, O. Terasaki, *Nature* **2006**, *444*, 79–81.

- [12] W. Wan, J. Sun, J. Su, S. Hovmöller, X. Zou, *J. Appl. Crystallogr.* **2013**, *46*, 1863–1873.
- [13] D. Zhang, P. Oleynikov, S. Hovmöller, X. Zou, *Z. Kristallogr.* **2010**, *225*, 94–102.
- [14] M. Gemmi, M. G. I. La Placa, A. S. Galanis, E. F. Rauch, S. Nicolopoulos, *J. Appl. Crystallogr.* **2015**, *48*, 718–727.
- [15] L. Xu, X. Ji, J.-G. Jiang, L. Han, S. Che, P. Wu, *Chem. Mater.* **2015**, *27*, 7852–7860.
- [16] Z. Liu, T. Ohsuna, O. Terasaki, M. A. Cambor, M.-J. Diaz-Cabanas, K. Hiraga, *J. Am. Chem. Soc.* **2001**, *123*, 5370–5371.
- [17] P. A. Wright, W. Zhou, J. Pérez-Pariente, M. Arranz, *J. Am. Chem. Soc.* **2005**, *127*, 494–495.
- [18] W. Wan, J. Su, X. D. Zou, T. Willhammar, *Inorg. Chem. Front.* **2018**, *5*, 2836–2855.
- [19] B. Shen, X. Chen, D. Cai, H. Xiong, X. Liu, C. Meng, Y. Han, F. Wei, *Adv. Mater.* **2020**, *32*, 1906103.
- [20] L. Liu, N. Wang, C. Zhu, X. Liu, Y. Zhu, P. Guo, L. Alfilfil, X. Dong, D. Zhang, Y. Han, *Angew. Chem. Int. Ed.* **2020**, *59*, 819–825; *Angew. Chem.* **2020**, *132*, 829–835.
- [21] R. L. Wadlinger, G. T. Kerr, E. J. Rosinski, US3308069, **1967**.
- [22] J. M. Newsam, M. M. J. Treacy, W. T. Koetsier, C. B. D. Gruyter, *Proc. R. Soc. London Ser. A* **1988**, *420*, 375–405.
- [23] J. B. Higgins, R. B. LaPierre, J. L. Schlenker, A. C. Rohrman, J. D. Wood, G. T. Kerr, W. J. Rohrbaugh, *Zeolites* **1988**, *8*, 446–452.
- [24] R. F. Lobo, M. Pan, I. Chan, H.-X. Li, R. C. Medrud, S. I. Zones, P. A. Crozier, M. E. Davis, *Science* **1993**, *262*, 1543–1546.
- [25] R. F. Lobo, M. Tsapatsis, C. C. Freyhardt, I. Chan, C.-Y. Chen, S. I. Zones, M. E. Davis, *J. Am. Chem. Soc.* **1997**, *119*, 3732–3744.
- [26] M. W. Anderson, O. Terasaki, T. Ohsuna, A. Philippou, S. P. MacKay, A. Ferreira, J. Rocha, S. Lidin, *Nature* **1994**, *367*, 347–351.
- [27] S. C. Weston, K. G. Strohmaier, H. B. Vroman, EP2817262, **2012**.
- [28] M. D. Shannon, *Proceedings from the Ninth International Zeolite Conference*, Elsevier, Amsterdam, **1993**, pp. 389–398.
- [29] S. C. Weston, B. K. Peterson, J. E. Gatt, W. W. Lonergan, H. B. Vroman, M. Afeworki, G. J. Kennedy, D. L. Dorset, M. D. Shannon, K. G. Strohmaier, *J. Am. Chem. Soc.* **2019**, *141*, 15910–15920.
- [30] J. Cho, Y. Yun, H. Xu, J. Sun, A. W. Burton, K. G. Strohmaier, G. Terefenko, H. Vroman, M. Afeworki, G. Cao, H. Wang, X. Zou, T. Willhammar, *Chem. Mater.* **2021**, *33*, 4146–4153; Correction: J. Cho, Y. Yun, H. Xu, J. Sun, A. W. Burton, K. G. Strohmaier, G. Terefenko, H. Vroman, M. Afeworki, G. Cao, H. Wang, X. Zou, T. Willhammar, *Chem. Mater.* **2021**, *33*, 6249.
- [31] W. Hua, H. Chen, Z.-B. Yu, X. Zou, J. Lin, J. Sun, *Angew. Chem. Int. Ed.* **2014**, *53*, 5868–5871; *Angew. Chem.* **2014**, *126*, 5978–5981.
- [32] Y. Xu, Y. Li, Y. Han, X. Song, J. Yu, *Angew. Chem. Int. Ed.* **2013**, *52*, 5501–5503; *Angew. Chem.* **2013**, *125*, 5611–5613.
- [33] D. Jo, Y. Zhang, J. H. Lee, A. Mayoral, J. Shin, N. Y. Kang, Y. Park, S. B. Hong, *Angew. Chem. Int. Ed.* **2021**, *60*, 5936–5940; *Angew. Chem.* **2021**, *133*, 6001–6005.
- [34] Y. Luo, S. Smeets, Z. Wang, J. Sun, W. Yang, *Chem. Eur. J.* **2019**, *25*, 2184–2188.
- [35] T. Willhammar, X. Zou, *Z. Kristallogr. - Cryst. Mater.* **2013**, *228*, 11–27.
- [36] I. Lazić, E. G. T. Bosch, S. Lazar, *Ultramicroscopy* **2016**, *160*, 265–280.
- [37] E. G. T. Bosch, I. Lazić, S. Lazar, *Microsc. Microanal.* **2016**, *22*, 306–307.
- [38] “DIFFaX software,” <http://www.public.asu.edu/~mtreacy/DIFFaX.html>.
- [39] P. S. Bárcia, F. Zapata, J. A. C. Silva, A. E. Rodrigues, B. Chen, *J. Phys. Chem. B* **2007**, *111*, 6101–6103.

Manuscript received: July 26, 2021

Accepted manuscript online: September 2, 2021

Version of record online: October 4, 2021